Upgrading of the 4.5 MV Dynamitron Accelerator at Tohoku University for Microbeam and Nanobeam Applications

II. 3. Upgrading of the 4.5 MV Dynamitron Accelerator at Tohoku University for Microbeam and Nanobeam Applications

Matsuyama S.[1], Ishii K.[1], Fujisawa M.[1], Kawamura Y.[1], Tsuboi S.[1], Yamanaka K.[1], Watanabe M.[1], Hashimoto Y.[1], Ohkura S.[1], Fujikawa M.[1], Nagaya T.[1], Komatsu K.[1], Yamazaki H.[2], and Kikuchi Y.[1]

[1]*Department of Quantum Science and Energy Engineering, Tohoku University*
[2]*Cyclotron and Radioisotope Center, Tohoku University*

Introduction

A 4.5 MV Dynamitron accelerator was constructed in 1974 for neutron and ion-beam experiments. The Dynamitron accelerator is a single-ended type with a Schenkel type high-voltage power supply. The accelerator was provided with a high-current duoplasmatron ion source, which can generate hydrogen, deuterium, or helium ion beams. The maximum beam current is greater than several hundred microamperes (3 mA recorded). A microbeam line was installed in July 2002[1)]; optimization of the system was performed. A beam spot of 0.4×0.4 μm^2 at a beam current of several tens of picoamperes has been produced and smaller beam spots are anticipated in the low-current regime[2)].

The analysis system has also been developed and is applicable to simultaneous in-air/in-vacuum PIXE, RBS, SE, and STIM analyses[2-4)] and 3D μ-CT[5-7)]. These applications demand beam currents of ca. 100 pA, which restricts the spatial resolution to around 1×1 μm^2. In addition, the beam current stability was insufficient. The beam brightness must be increased to improve the resolution to several hundreds of nanometers in the analysis.

In this study, the terminal equipment and an acceleration tube of the Dynamitron accelerator were upgraded to improve the beam brightness and decrease the beam spot size to several tens of nanometers with sufficient beam current for analyses.

System Description

Terminal equipment

The terminal equipment comprises a duoplasmatron ion source along with an extractor,

an Einzel lens, an E×B filter, a pulsing system, and a gap lens. The system configuration is almost identical to the previous one. The ion source, lens system, and their control system are shown in Figure 1. The vacuum products were provided by National Electrostatics Corporation (NEC). The ion source is expected to produce ca. 10 mA H_1^+ beams, with beam emittance of 2.1 mm· mrad· $MeV^{1/2}$ (specification). Both values are better than those of the previous ion source. Moreover, they are estimated to be brighter than other RF ion sources. An uncoated tungsten filament (0.9 mm diameter) was obtained from NEC. The tungsten filament lifetime was too short, only several hours, which is unsuitable for an ion source used in the single-ended accelerator. Therefore, a LaB_6 filament (C2B, Denka Co. Ltd.) was used to achieve a longer lifetime. A 0.1-mm-diameter anode aperture made of iron was also supplied by NEC. The aperture was obstructed within several hours because of the heat load in the source. As the previous ion source, we had used a 0.3-mm-diameter tungsten anode aperture. The aperture can be used for more than 10,000 h without deterioration. Therefore, we used a 0.3 mm diameter anode aperture lined with tungsten. The extracted beams pass through the Einzel lens and the E×B filter. An electrical field E, formed by a deflector and a magnetic field B by permanent magnets, is crossed in the E×B filter. Under the combined influence of E and B, the net force on the particles is cancelled at the specific mass, charge, and velocity conditions. Then the E×B filter provides mass analysis of a monoenergetic beam by selecting a deflection voltage. The Einzel lens focuses the beam on the E×B aperture (1.5 mm diameter). Because the beam spot size on the aperture influences the ability of mass analysis, the Einzel lens performance is important. The duoplasmatron ion source generates more than one ion species. In case of generating hydrogen plasma, the source will produce not only protons, but also diatomic and triatomic molecular hydrogen as well as minor amounts of other ion species. Therefore, the E×B filter reduces the load to the accelerator and improves the accelerator stability. The gap lens focuses the beam to match beam parameters into the acceleration tube[8]. Although the system includes a sweep, a pop, and a buncher for pulsed beam production, their power supplies are not equipped. In this study, the sweep electrodes are used as a steerer by DC voltage application.

The whole control system was developed by our group. The system configuration is presented in Figure 1. These power supplies are driven by 0–10 V signals from digital-to-analog converters (DACs) and are monitored using analog-to-digital converters (ADCs) in programmable logic controllers (PLC, FA-M3; Yokogawa Electric Corp.). The DAC and ADC modules are standard components of the PLC, but special modifications were

undertaken for spark protection. These PLCs in the terminal (sub PLC units) have no CPU and are connected to a main PLC in the ground potential via two plastic fibers. The main PLC module has CPU, receives commands from a personal computer and controls the sub PLC units in the terminal. The main PLC module was used outside an accelerator pressure tank to prevent damage caused by spark-out. In this case, the plastic fibers must traverse the pressure tank. Because the plastic fiber is colored by X-ray irradiation, it must be changed periodically. For easy fiber maintenance, light signals are converted to electric signals, extracted as electric signals through hermetic connectors, then reconverted to light signals using light/signal converters that were specially developed by our group.

The control parameters for operation are stored in the memory space of the main PLC. A personal computer used as the user interface can only refer to these parameters via an Ethernet network. During the start-up process, control software retrieves the parameters for the PLC and can send commands to change the parameters. This framework was adopted to address the situation of a possible computer hang-up. Control software was designed using LabVIEW based on user requirements and requests.

Acceleration tube

The acceleration tube was replaced with a new one obtained from NEC. The acceleration tube comprises 12 sections arranged in compressed geometry. Figure 2 portrays schematic drawings of one section of the tube. The acceleration tube was assembled in one piece compressed with two square flanges and four Lucite tension rods and was shipped in one piece. Each section has 18 live gaps and 3 shorted gaps. The center of the shorted region has an aperture of 25.4 mm diameter and internal electrodes, which resemble those between the sections. The lens effect will be stronger than that of the previous tube, which has larger apertures. The potential grading of the tube is provided with high mega-ohm resisters. The first seven gaps of the tube have lower value resistors (60 MΩ) than the other 209 gaps (100 MΩ). The gradient is lower in the first gaps. For that reason, the strength of the entrance lens effect is reduced, which better matches the available gap lens voltages.

Performance of the system

1. Basic performance

Upgrading of the accelerator started February 2007 and the first beam was obtained August 2007. First, high-voltage spark-out of the accelerator damaged the terminal

equipment. By adding filters and shields, damage to the equipment was reduced. Figure 3 shows a typical mass spectrum measured at a 0 deg target by varying the voltage to the ExB filter. The H_1^+, H_2^+, and H_3^+ beams were sufficiently separated and the ExB filter functioned as expected. Because the data were measured at an arc current of 0.5 A, the proton ratio is ca. 0.15, which is rather low. Maximizing the proton ratio necessitates maximizing the arc current and minimizing the source gas pressure. However, a tradeoff pertains between low source gas pressure and source stability. High arc currents are great for a high proton ratio, but take the risk of welding the anode aperture shut. From these conditions, we are running the source for the arc current range of 1–2 A for proton beam production. The gas pressure is used at the lowest level where the source works stably. Even in that condition, the proton ratio is ca. 0.25, which is lower than that from operational experience of the same NEC duoplasmatron ion source[9].

The beam current was measured at the 0 deg target. Proton beam currents of 21 μA, 52 μA, and 75 μA were obtained respectively for arc currents of 1.0, 1.5, and 2 A with a 0.25 A magnet current. Because the source is expected to provide more than 1 mA of H^+ beam, beam currents were lower than expected. By applying the voltage to the sweep and increasing the magnet current, the beam current increased and exceeded 100 μA at an arc current of 2 A. The beam shifts by varying ion source parameters. Misalignments might occur in the ion source and lens system in the terminal. For H_2^+, the beam currents of 100 μA were obtained easily with lower arc current, which might be related to the lower proton ratio. Additional adjustments for ion source geometry and for operational conditions should be made to improve the performance.

The lifetime of a LaB_6 filament in the source is longer 700 h; it is still running. The aperture lined with tungsten has worked for more than 900 h without changing beam properties. The accelerator has been operated routinely for various experiments without a serious problem.

2. Beam brightness

The beam brightness is of primary importance to focus the beam down to micrometer scale with sufficient beam current. The system's beam brightness was measured by measuring the target current in the microbeam system for 2.4 MeV hydrogen beams. The microbeam system consists of a doublet quadrupole and the slit-system of microslits (MS), divergence-defining slits (DS), and baffle slits (BS)[1,2]. The brightness was measured using

various DS slit width in square geometry. The MS widths were set at 82×12 μm^2, which correspond to beam spot size of 1.5×1.5 μm^2.

As described by Liouville's theorem[10], the beam brightness cannot be increased using a subsequent optical system. It can only decrease according to effects such as those of collimation and misalignment. Beam lines to the microbeam system are short and simple in the newly built facilities for nanobeam and microbeam applications. However, our microbeam system is sufficiently long to reduce the beam brightness because the system is connected to the existing beam line and to a high-resolution beam-energy analyzing system[1]. Figure 4 shows the beam line to the microbeam system. Accelerated beams pass through a doublet quadrupole lens (DQ1), a switching magnet, another quadrupole doublet lens (DQ2) and the analyzing system and enter the microbeam system. To define the correct axis with respect to the analyzing magnet and to keep the energy analyzing performance, DQ2 was not used in the normal operation. The highest beam brightness of the previous system was ca. 0.7 $pA \cdot \mu m^{-2} \cdot mrad^{-2} \cdot MeV^{-1}$ at a half divergence of 0.2 mrad. In this study, the brightness was measured for three beam transport conditions. Figure 4 presents the calculated beam envelope after passage through the ExB aperture to the entrance of the energy analyzing system using OPTICSIII code, which is supplied from NEC for three beam transport conditions. The first condition (case 1), higher extraction voltage (ca. 30 kV) and higher gap lens voltage (ca. 55 kV), was applied and DQ1 was used. These voltages and currents of the lens system were adjusted to obtain the highest beam current at the target. Using higher extraction and gap lens voltage, the lens effect of the tube is the weakest. Therefore, the accelerated beams are estimated as parallel beams. For case 2, the standard extraction voltage (20 kV) was applied. The gap lens voltage was arranged such that the waist was formed in the tube exit. Both DQ1 and DQ2 were used in this case. Case 2 is the highest beam transmission in the accelerator and is recommended from NEC. For case 3, the standard extraction voltage (20 kV) and lower gap lens voltage (10 kV) were applied; only DQ1 was used. In this setting, the beam waist is formed in the middle of the tube and the transmission in the accelerator is not good. Figure 5 portrays the measured beam brightness for three beam transport conditions with that obtained using the previous system. The beam brightness in case 2 is 0.7 $pA \cdot \mu m^{-2} \cdot mrad^{-2} \cdot MeV^{-1}$ at a half divergence of 0.1 mrad; it is highest in these cases, but is lower than that of the previous system. As shown in the beam envelope calculation, the beam spot size at entrance slit of the energy analyzing system (ESS1, slit opening = 0.4 mm) is smallest in case 2; thereby, the beam brightness is highest. As mentioned in this section,

chromatic aberration may increase in case 2. Thus the beam transport condition of case 2 is applicable to an experiment with a beam spot size larger than 1×1 μm^2. The beam brightness of case 1 is almost identical to that of case 3. In case 1, the beam brightness increased with the slit opening of ESS1. The slit opening of ESS1 affects the energy resolution. The beam brightness increased by five times, as expected from energy stability of the accelerator when the slit opening is set to 5 mm[1)].

To compare brightness among various systems, a brightness value at 0.07 mrad half divergence is used as a normalized brightness[11-13)]. The highest normalized brightness was reported as 30 $pA \cdot \mu m^{-2} \cdot mrad^{-2} \cdot MeV^{-1}$ [11)]. The value of 74 $pA \cdot \mu m^{-2} \cdot mrad^{-2} \cdot MeV^{-1}$ was reported in a different half divergence[14,15)]. Normalized beam brightness of 0.44 $pA \cdot \mu m^{-2} \cdot mrad^{-2} \cdot MeV^{-1}$ was obtained in case 1, which was obtained under the arc current of 1.8 A and magnet current of 0.3 A. Under these conditions, the source provided 45 μA H^+ beam. For H_2^+ beams, normalized brightness of 2.6 $pA \cdot \mu m^{-2} \cdot mrad^{-2} \cdot MeV^{-1}$ was obtained. This value was obtained under the arc current of 0.6 A and magnet current of 0.3A. The source provided 120 μA H_2^+ beam. As described in the preceding section, adjustment of the ion source is not perfect and the beam current and proton ratio are lower than expected. The brightness is improved with adjustment of the source. Because the anode aperture diameter also affects the brightness, aperture optimization should also be done.

3. High-voltage stability

The beam current of the previous system fluctuated between 0 and its maximum value, which stemmed from the instability of the terminal voltage. The voltage ripple was sometimes larger than 10^{-3} and was larger than the specification. Voltage ripple of this order can be measured easily using the load current change of the resisters, which were connected from the terminal to the ground (high voltage divider, HVD). After replacing the tube, the voltage ripple was measured, but it did not decrease drastically. The voltage ripple came from bad adjustment of the voltage regulation circuit. A proportional integration (PI) regulator is used to stabilize the high voltage. The PI controller acts on the error signal from the comparison of the set reference voltage and the voltage generated on the precise resister by the HVD current. The response time is very important to stabilize the terminal voltage. The response time was adjusted at installation of the accelerator when rectifier tubes were used for high voltage generation. After changing the rectifier tube into diodes, readjustment was not carried out. Readjustment should be carried out because the response of the diodes is faster

than that of the rectifier tubes. Because voltage stability was not important for any application at that time, adjustment was not carried out. After adjusting the response time, the voltage ripple decreased to a level that was within the specification, thereby improving the beam current stability at the microbeam target. The elemental map had an artifact that was attributed to the beam current fluctuation in the previous system. After upgrading the system and adjusting the response, the artifact was greatly reduced. As the next step, we are planning to replace the voltage regulating system and to increase the system performance.

Conclusion

The Dynamitron accelerator at Tohoku University was upgraded to improve the microbeam performance and decrease the beam spot size down to several tens of nanometers with beam currents of ca. 100 pA. The microbeam system has the capability of focusing the beam down to several hundred square micrometers, but beam currents were insufficient for analyses at sub-micrometer resolution.

An ion source and lenses in the terminal and an acceleration tube were replaced with new ones from National Electrostatics Corporation. The control system of the terminal equipment was also developed by our group. Beam brightness of 2.6 and 0.44 $pA \cdot \mu m^{-2} \cdot mrad^{-2} \cdot MeV^{-1}$ was obtained for H_2^+ and H_1^+ beams at a half divergence of 0.07 mrad. The beam brightness is lower than expected and optimization of the ion source and its operational condition should be carried out. The voltage stability of the accelerator was improved by adjusting the voltage stabilizing system. Thereby, the beam current stability is improved and artifact shown in the elemental image was greatly reduced. The Dynamitron accelerator has been operated routinely for various experiments without a serious problem and will be useful for nanobeam and microbeam applications.

Acknowledgements

The authors thank Prof. M. Igashira, Tokyo Institute of Technology, Dr. T. Matsumoto, National Institute of Advanced Industrial Science and Technology, and Dr. M. Kowatari, Japan Atomic Energy Agency for their valuable suggestions and advice from their experience on their duoplasmatron ion source of the Pelletron accelerator. The authors also acknowledge the assistance of Dr. C. Kobayashi, Dr. T. Yoshida, Mr. S. Takahashi, Mr. M. Anshita, and Mr. T. Saito (Staff of Hakuto Co. Ltd.) in installing the ion source and the acceleration tube.

This study was partly supported by Grants-in-Aid for Scientific Research, (S) No. 13852017, (B) No. 18360450, (C) No. 16560731, and a Grant-in-Aid for Scientific Research

in Priority Areas under Grant No. 14048213 from the Ministry of Education, Culture, Sports, Science and Technology, Japan.

References

1) Matsuyama S., Ishii K., Yamazaki H., Sakamoto R., Fujisawa M., Amartaivan Ts., Ohishi Y., Rodriguez M., Suzuki A., Kamiya T., Oikawa M., Arakawa K., Matsumoto N., Nucl. Instr. andMeth. **B210** (2003) 59.
2) Matsuyama S., Ishii K., Yamazaki H., Kikuchi Y., Inomata K., Watanabe Y., Ishizaki A., Oyama R., Kawamura Y., Yamaguchi T., Momose G., Nagakura M., Takahashi M., Kamiya T., Nucl. Instr. Meth. Phys. Res. **B260** (2007) 55.
3) Matsuyama S., Ishii K., Yamazaki H., Barbotteau Y., Amartaivan Ts., Izukawa D., Hotta K., Mizuma K., Abe S., Oishi Y., Rodriguez M., Suzuki A., Sakamoto R., Fujisawa M., Kamiya T., Oikawa M., Arakawa K., Imaseki H., Matsumoto N., Int. J. of PIXE, **14** (1&2) (2004) 1.
4) Matsuyama S., Ishii K., Abe S., Ohtsu H., Yamazaki H., Kikuchi Y., Amartaivan Ts., Inomata K., Watanabe Y., Ishizaki A., Barbotteau Y., Suzuki A., Yamaguchi T., Momose G., Imaseki H., Int. J. of PIXE, **15** (1&2) (2005) 41.
5) Ishii K., Matsuyama S., Yamazaki H., Watanabe Y., Yamaguchi T., Momose G., Amartaivan Ts., Suzuki A., Kikuchi Y., Galster W., Int. J. of PIXE, **15** (3&4) (2005) 111.
6) Ishii K., Matsuyama S., Yamazaki H., Watanabe Y., Kawamura Y., Yamaguchi T., Momose G., Kikuchi Y., Terakawa A., Galster W., Nucl. Instr. and Meth. **B249** (2006) 726.
7) Ishii K., Matsuyama S., Watanabe Y., Kawamura Y., Yamaguchi T., Oyama R., Momose G., Ishizaki A., Yamazaki H., Kikuchi Y., Nucl. Instr. and Meth. **A571** (2007) 64.
8) Elkind M.M., Rev. of Sci. Instr., **24** (1953) 129.
9) Igashira M., private communication.
10) Grime G.W., Watt F., "Beam Optics of Quadrupole Probe-forming Systems," Adam Hilger Ltd, Bristol (1984).
11) Szymanski R., Jamieson D.N., Nucl. Instr Meth. **B130** (1997) 80.
12) Rout B., Greco R., Pastore N., Dymnikov A.D., Glass G.A., Nucl. Instr. Meth. **B241** (2005) 382.
13) Jamieson D.N., Rout B., Szymanski R., Spizzirri P., Sakellarieu A., Belcher W. Ryan C.G., Nucl. Instr. Meth. **B190** (2002) 80.
14) Visser J., Mous D.J.W., Gottdang A., Haitsma R.G., Nucl. Instr. Meth. **B231** (2005) 32.
15) Watt F., van Kan J.A., Rajta I., Bettiol A.A., Choo T.F., Breese M.B.H., Osipowicz T., Nucl. Instr. Meth. **B210** (2003) 14.

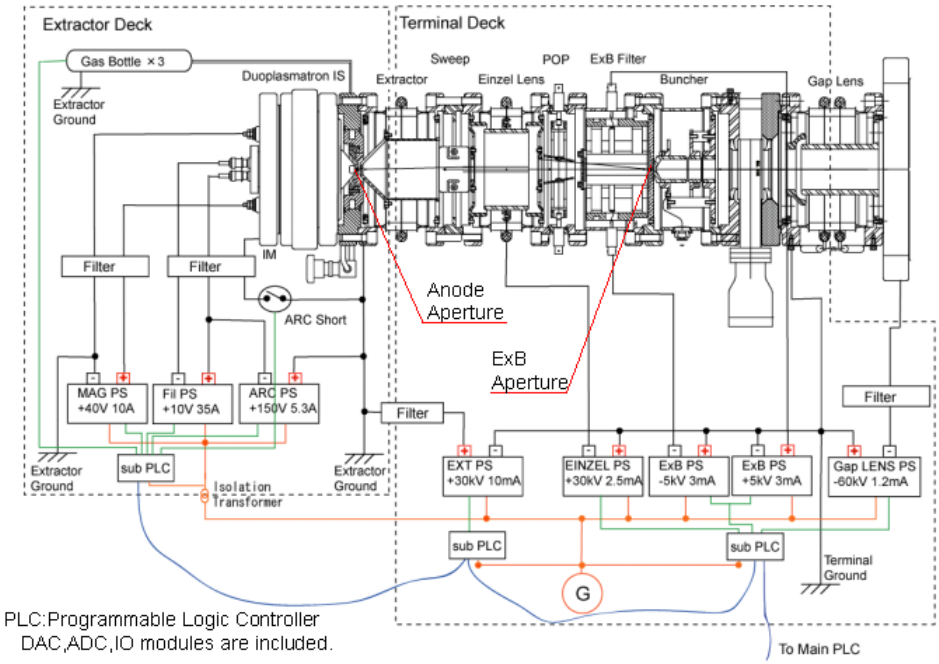

Figure 1. Schematic diagram of the ion source, lens, and control system.

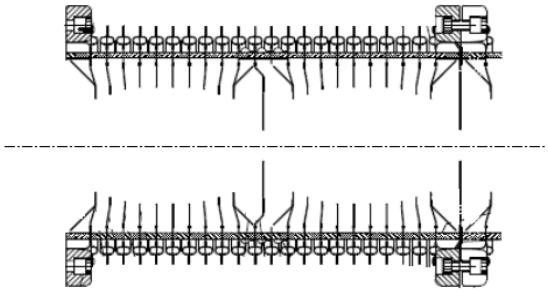

Figure 2. Schematic diagram of the acceleration tube.

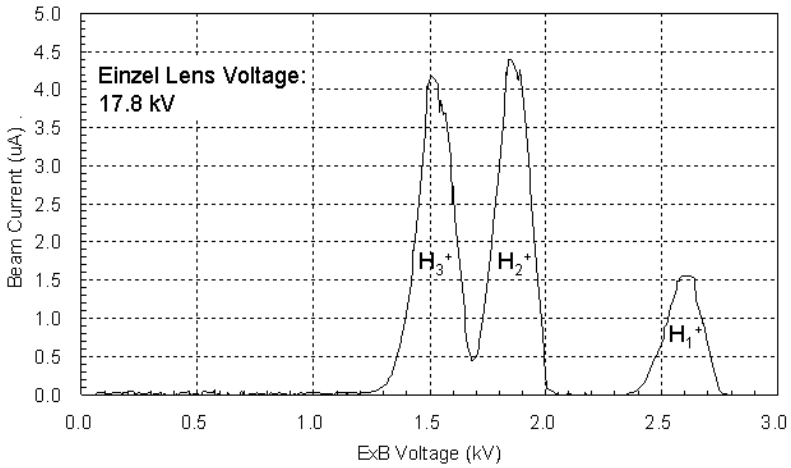

Figure 3. Mass spectrum measured by varying the voltage applied to E×B filter at the 0-deg target.

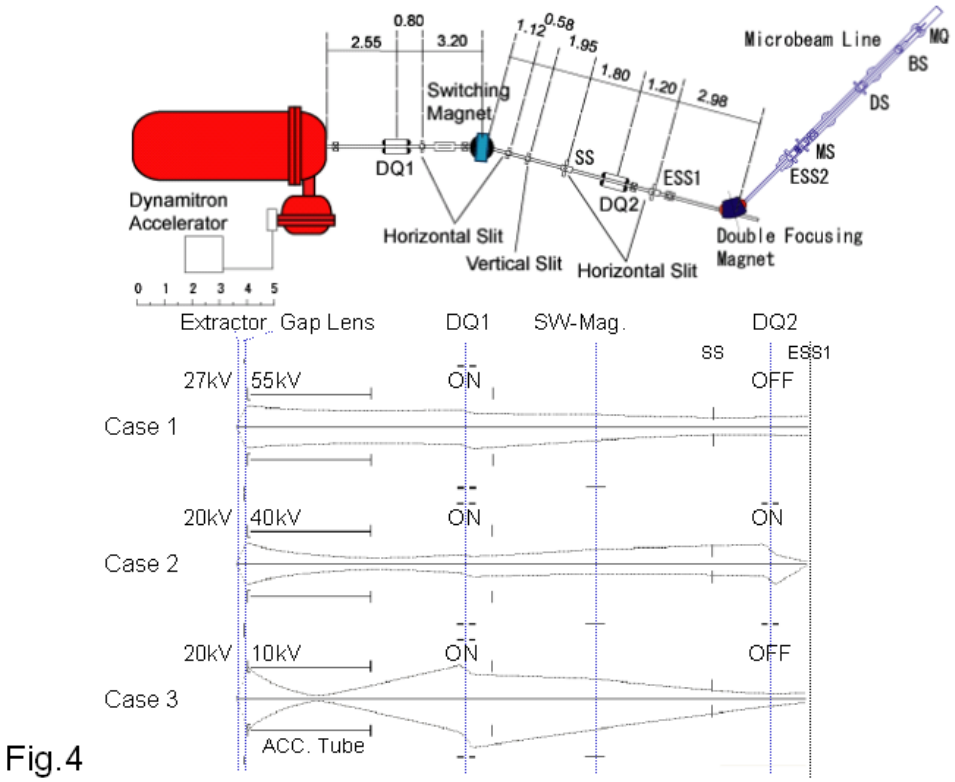

Fig.4

Figure 4. Beam transport system and beam envelope calculated using OPTICSIII from NEC for three transport conditions.

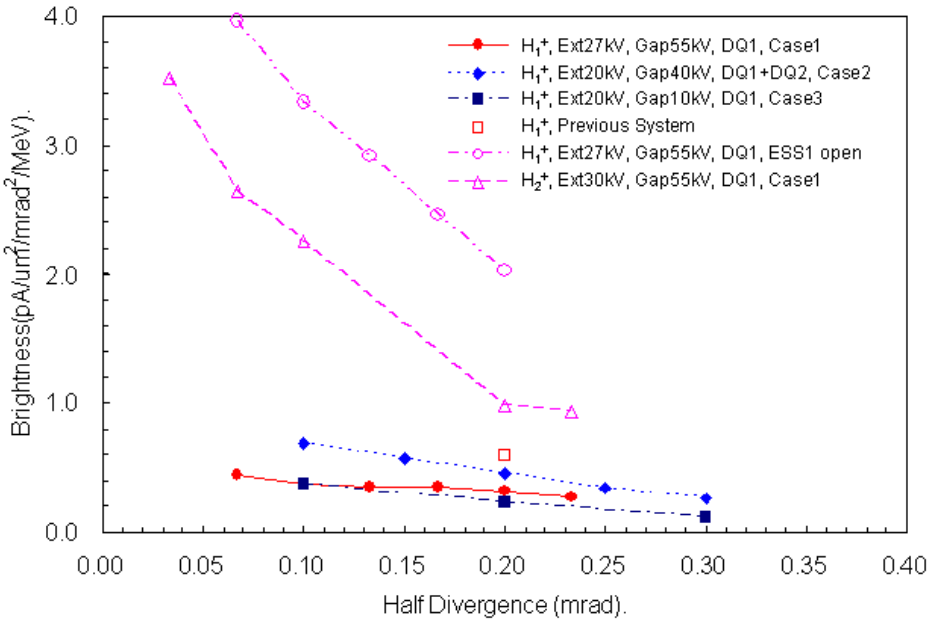

Figure 5. Measured beam brightness for three beam transport conditions.